ETH zürich

ETH Library

Carbonatitic dykes during Pangaea transtension (Pelagonian Zone, Greece)

Journal Article

Author(s):
Schenker, Filippo L.; Burg, Jean-Pierre; Kostopoulos, Dimitrios; Baumgartner, Lukas P.; Bouvier, Anne-Sophie

Publication date:
2018-03

Permanent link:
https://doi.org/10.3929/ethz-b-000258126

Rights / license:
Creative Commons Attribution-NonCommercial-NoDerivatives 4.0 International

Originally published in:
Lithos 302-303, https://doi.org/10.1016/j.lithos.2018.01.011

This page was generated automatically upon download from the ETH Zurich Research Collection.
For more information, please consult the Terms of use.

Lithos 302–303 (2018) 329–340

Contents lists available at ScienceDirect

Lithos

journal homepage: www.elsevier.com/locate/lithos

Carbonatitic dykes during Pangaea transtension (Pelagonian Zone, Greece)

Filippo Luca Schenker [a,b,c,*], Jean-Pierre Burg [b], Dimitrios Kostopoulos [d], Lukas P. Baumgartner [c], Anne-Sophie Bouvier [c]

[a] Institute of Earth Sciences, University of Applied Sciences and Arts of Southern Switzerland, SUPSI, Canobbio, Switzerland
[b] Geological Institute, ETH Zurich, Zurich, Switzerland
[c] Institute of Earth Sciences, University of Lausanne, Lausanne, Switzerland
[d] School of Science, Faculty of Geology and Geoenvironment, National and Kapodistrian University of Athens, Greece

ARTICLE INFO

Article history:
Received 9 May 2017
Accepted 13 January 2018

Keywords:
Carbonatite
fenite
Pelagonia
Pangaea
Permian
Tethys
Variscan

ABSTRACT

Carbonatitic dykes surrounded by K-Na-fenites were discovered in the Pelagonian Zone in Greece. Their carbonate portions have an isotopic mantle signature of $\delta^{13}C$ and $\delta^{18}O$ ranging from −5.18 to −5.56 (‰ vs. VPDB) and from 10.68 to 11.59 (‰ vs. VSMOW) respectively, whereas their mafic silicate portions have high Nb, Ta and ε_{Nd} values, typical of alkaline basalts. Textural relationships hint at a cogenetic intrusion of silicate and carbonate liquids that according to antithetic REE profiles segregated at shallow depths (<0.6 GPa) from a parental melt sourced deeper in the mantle. Fenites bear similar REE abundances to mafic rocks but with high Rb-Ba and low Nb-Ta values. SHRIMP II U-Pb analyses of magmatic zircon cores ($\delta^{18}O = 7.21–7.51$) from a carbonate-bearing syenitic amphibolite yielded a Permian intrusion age at 278 ± 2 Ma, considerably older than a Cretaceous (118 ± 4 Ma) greenschist overprint obtained from metamorphic zircon rims ($\delta^{18}O = 6.78–7.02$).
From 300 to 175 Ma the ε_{Nd} of the Pelagonian magmatism rose irregularly to more primitive values attesting to a higher increment of asthenosphere-derived melts. In this context, the carbonatite formed within a transtensional regime of an intra-Pangaea dextral transform fault that signalled the forthcoming penetrating breakoff of the supercontinent, manifested in the Permo-Triassic.
© 2018 The Authors. Published by Elsevier B.V. This is an open access article under the CC BY-NC-ND license (http://creativecommons.org/licenses/by-nc-nd/4.0/).

1. Introduction

Carbonatites are carbonate-rich magmatic rocks (e.g. Streckeisen, 1980) genetically linked to suites of alkaline rocks, in places ranging from ultramafitites to syenites (e.g. Egorov, 1970; Kogarko and Zartman, 2007). Judging from their widespread presence in continental extensional settings (e.g. Woolley, 1989), carbonatites are generally regarded as deep melts rising from the mantle (e.g. Wyllie, 1989). Geochemical evidence of carbonatites in other settings such as ocean islands, transcrustal shear zones and subduction zones point to a similar mantellic origin (e.g. Rajesh and Arai, 2006; Walter et al., 2008; Woolley et al., 1991). Intrusions and eruptions of carbonatites play an important role in the global carbon cycle (Patterson and Francis, 2013) because they are considered to vent the CO_2 stored in the mantle into the crust and the atmosphere (Coltice et al., 2004). Their importance is mostly related to economic geology since they often contain high concentrations of rare-earth elements (REE; Cullers and Graf, 1984; Yang et al., 2011).

Three petrogenetic models of carbonatitic magma generation have been proposed (see Jones et al., 2013 for a review): (i) Primary melts from low degree of partial melting of carbonated, hydrous peridotite (e.g. Falloon and Green, 1989); (ii) Differentiated melts from fractional crystallization in CO_2-bearing silicate melts (e.g. Watkinson and Wyllie, 1971); (iii) Immiscible melts separated at depth from a CO_2-saturated (e.g. Freestone and Hamilton, 1980; Kjarsgaard and Hamilton, 1988) but also CO_2-undersaturated silicate melt (e.g. Brooker and Kjarsgaard, 2011). Hybrid models have also been proposed (e.g. Kjarsgaard and Hamilton, 1988). Carbonatites are geochemically characterized by high concentrations of light REE (LREE), Sr, Ba, and P (e.g. Nelson et al., 1988). Alkali-rich (Na, K) carbonatites are rare (Woolley and Kjarsgaard, 2008). Nevertheless, carbonatites are usually surrounded by alkaline metasomatic rocks (mostly Na-rich fenites) attesting that carbonatitic melts bear alkalis that they give off during cooling and crystallization (e.g. Kjarsgaard and Hamilton, 1988; Le Bas, 1981, 2008). It is important to note that carbonatites show a considerable variation at different scales in modal mineralogy, and in major- and trace-element composition, depending on the stage of crystallization, melt or fluid segregation and percolation (e.g. Chen and Simonetti, 2013; Weidendorfer et al., 2016; Xu et al., 2011; Xu et al., 2015). Many compositions may hence differ from

* Corresponding author at: Institute of Earth Sciences, University of Applied Sciences and Arts of Southern Switzerland, SUPSI, Canobbio, Switzerland.
E-mail address: filippo.schenker@supsi.ch (F.L. Schenker).

https://doi.org/10.1016/j.lithos.2018.01.011
0024-4937/© 2018 The Authors. Published by Elsevier B.V. This is an open access article under the CC BY-NC-ND license (http://creativecommons.org/licenses/by-nc-nd/4.0/).

those carrying diagnostic carbonatitic signatures. As a result, a complete examination taking into account carbonatites, associated alkaline suites and metasomatic country rocks is required to fully characterize carbonatites.

It follows that, identifying carbonatites in orogenic segments remains a challenge because of the tectonic fragmentation of the carbonatite-alkaline magmatic edifice and the effects of metamorphism and metamorphic fluids. In addition, metacarbonatites can have similar geochemical features to marble or deep-seated carbonate fluids (e.g. Le Bas et al., 2002) or skarn-related carbonates (e.g. Lentz, 1999). In this study, we use a multi-disciplinary approach combining geology, structures, petrology, geochemistry (including isotopes) and zircon U-Pb geochronology to document the occurrence of a hitherto unidentified Permian carbonatite (now exposed as boudinaged carbonatitic dikes) intruded in the Variscan basement of Greece, which has been metamorphosed during the Cretaceous. Our discovery, along with consanguineous rocks of Lower Carboniferous age reported from localities nearby in Bulgaria (Dyulgerov et al., 2010), demonstrates an important rise of the lithosphere-asthenosphere boundary in that part of Pangaea from the Lower Carboniferous to Triassic, and underscores the critical role of enrichment processes in preconditioning the continental lithosphere for rifting. Similar conclusions have recently been reached for the break-up of the North Atlantic Craton (Tappe et al., 2017). All analytical methods and tables are described in the Appendix A.

2. Tectonic and geological setting

The study area is situated in the Hellenide mountain chain of NW Greece and refers to a carbonate-amphibolite-epidotite rock-association occurring in the Pelagonian Zone, in the footwall of the Axios/Vardar/Almopias Zone (AVAZ) Suture (Fig. 1). The Pelagonian Zone has a polymagmatic history recorded in its crystalline basement dominated by Permo-Carboniferous metagranitoids that intruded into Proterozoic ortho- and paragneisses and are intruded themselves by Permian and Triassic felsic and mafic dykes (Anders et al., 2006; Anders et al., 2007; Pe-Piper, 1998; Reischmann et al., 2001; Schenker et al., 2014; Zlatkin et al., 2017). In the studied area, fragmented, fossil-devoid mylonitic marbles rest on the gneissic basement (Fig. 1b). Stratigraphic correlations with northwest Pelagonia suggest a late Palaeozoic to mid-Mesozoic age for this carbonate cover (Mercier, 1968; Mountrakis, 1986; Sharp and Robertson, 2006) testifying that Pelagonia was part of the Permian-Early Jurassic continental margin of the AVAZ basin and its seaways (Jacobshagen et al., 1978). Pelagonia has been accreted to the hanging wall of the Tethys subduction zone during the Late Jurassic-Cretaceous (e.g. Ricou et al., 1998) between the External Hellenides to the southwest and the Rhodope Metamorphic Province to the northeast (Fig. 1).

Structurally, the Pelagonian Zone is a wide, low-amplitude anticlinorium (Kilias et al., 2010). Two regional thermo-tectonic events were identified (Nance, 1981; Schenker et al., 2015): an early Cretaceous amphibolite- to greenschist-facies metamorphism (Lips et al., 1998; Schenker et al., 2014; Yarwood and Dixon, 1977) and an Eocene blueschist-facies metamorphism to the south (Godfriaux et al., 1988; Lips et al., 1998; Schermer, 1990; Schermer et al., 1990).

3. Field occurrence and petrology

An association of amphibolite, epidotite and carbonate was discovered in the Pelagonian basement, structurally below mylonitic marble (Fig. 1b). Phyllonites exhibiting top-to-the-SW shear bands occur between mylonitic marble and basement gneiss. The amphibolite-epidotite-carbonate rock association is wrapped by mylonitic gneisses, the whole lying within the regional main foliation. The gneisses are locally interlayered with micaschists. The studied carbonates were found within: (i) a ca. 200-m-long mafic boudin (Figs. 1b and 2a), (ii) ca. 1-m-thick mafic dykes (Fig. 2b) and (iii) ca. 1-m-long mafic lenses. The carbonates are both truncating (Fig. 2a) and included as clasts (Fig. 2c) into the boudinaged carbonate-bearing mafic rocks, suggesting that the viscosities of both liquids were close to each other with local variations. In magmatic systems, such field observations argue in favour of a cogenetic relationship between the two magmas. These primary structures, in the mafic rocks, are partially preserved within boudins and dykes, where they were protected from later deformation expressed by the wrapping regional foliation. Apart from the local presence of a-few-mm-thick secondary carbonate veins crosscutting the mafic rocks and the regional foliation in the country rock, no similar carbonate rock was found in the surrounding gneiss. The late carbonate veins reflect percolation of post-magmatic, post-foliation fluids. These observations confirm that (i) the locally boudinaged mafic-carbonate rock association intruded into the gneissic basement as dykes and (ii) a chemically closed carbon system existed within the boudins, dykes and lenses, independent of magmatic/fluid processes that took place in the surrounding rocks.

Three end-member rock types were distinguished in the mafic layers: Amphibolite, epidotite and carbonates; they are described in detail below. Transitional rock types such as epidote-amphibolite, amphibole-epidotite, etc. were also observed. Mineral analyses are listed in Appendix B.

(i) Amphibolites

Amphibolites (Fig. 2, sample P12-004 and P12-031) contain amphibole (modal proportion 90-50 v.%), epidote (40-5 v.%), titanite (5-1 v.%), calcite (5-2 v.%) and fluorapatite (1 v.%) as main mineral phases; biotite and zircon are accessories. Amphibole is zoned and exhibits intergranular or poikiloblastic overgrowth including epidote, calcite and titanite. Epidote and epidote aggregates display metamict cores diagnostic of allanite. Rare, up to 10 cm long idiomorphic fluorapatite crystals are in textural contact with amphibole (Fig. 2d) and calcite. Titanite appears as idiomorphic inclusions in amphiboles and in calcite or as elongated aggregates in the matrix. Biotite occurs as inclusions in amphibole and in calcite. In one locality, the amphibolite contains a ca. 1-cm-thick layer of amphibole-paragonite-white mica schist attesting to the presence of alkalis segregated from the mafic rock portion (Fig. 2e).

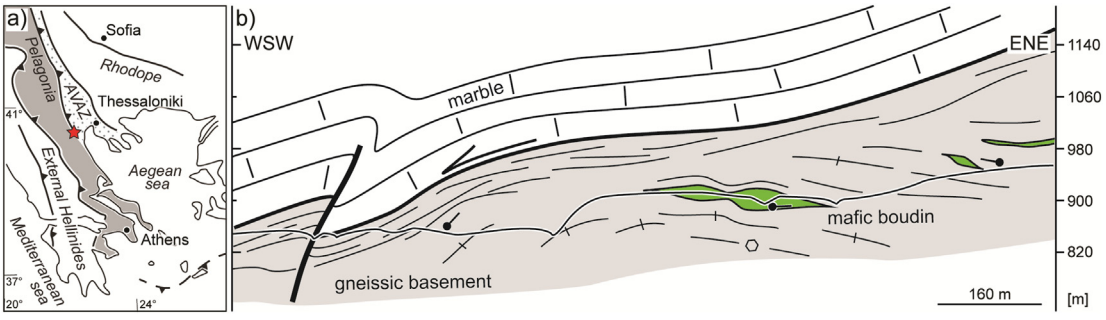

Fig. 1. a) Location of the Pelagonian zone in the Hellenides. AVAZ = Axios/Vardar/Almopias zone, Red star = studied area. b) Geological profile showing the tectono-stratigraphic position of the mafic lens and dykes containing the carbonates.

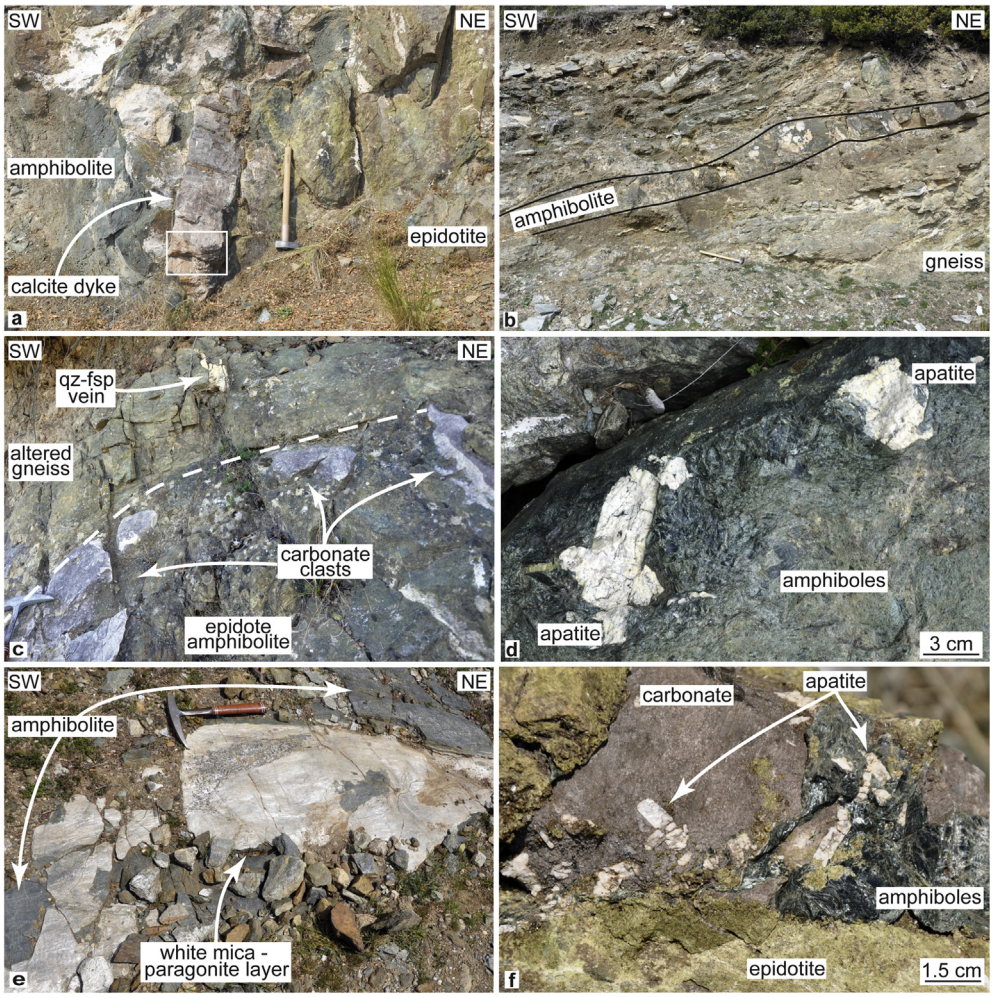

Fig. 2. Textural aspects of the carbonate-bearing amphibolite/epidotite rocks and country rock. (a) monocrystalline calcitic vein cutting the amphibolite and epidotite, framed = Fig. 6a. (b) Carbonate bearing-amphibolitic dyke. (c) Contact between gneissic country rock and carbonate-mafic rocks. Note that unlike sub-Fig. (a) the carbonate forms clasts in the mafic rock. (d) Ca. 10 cm long fluorapatite crystals in amphibolite. (e) Ca. 1 cm thick white mica-paragonite glimmerite within amphibolites. The Na and K of the glimmerite was probably released during crystallisation of the carbonatitic melts. (f) Ca. 1 cm long fluorapatite crystals in carbonates.

The amphibole composition varies from tremolite in the rims to hornblende-edenite in the cores (Fig. 3a). Sodium in the A site (Na^A, i.e. the alkali site occupancy representing the temperature-sensitive edenite component) is higher in the core than in the rims (Fig. 3b), reflecting either a more primitive Na-rich composition or growth during cooling or recrystallization/re-equilibration in a subsequent, lower-temperature thermal event. Amphiboles in carbonatites show a wide range of compositions and are not necessarily alkaline (Reguir et al., 2012); the composition of the core of the Pelagonian amphiboles plots between the composition of Ca-amphiboles of the Pinghe carbonatites and the Al-poor Ca-Na amphibole of the Afrikanda carbonatites. Epidote is characterized by a high FeO_{tot} content (12.72–12.89 wt.%) without compositional zoning. Epidote, especially allanite, occurs frequently in old metamorphosed carbonatites (e.g. Moecher et al., 1997).

(ii) Epidotites

Epidotites (Fig. 2a, sample P12-033) are composed of epidote (95-50 v.%), amphibole (15-5 v.%), calcite (10-1 v.%), titanite (1-3 v.%), diopside (10-1 v.%), garnet (10-1 v.%) and biotite (1 v.%). Unidentified opaque minerals are accessories. Epidote forms a fine-grained, light-green matrix with patches of carbonate. Amphibole is either sub-idiomorphic showing poikiloblastic texture (including the epidote) or xenomorphic in epidote aggregates. Garnet cores include chromite and unidentified brown (in transmitted light) inclusions. Garnet, locally associated with diopside, shows minor zoning in Ca (grossular component from 0.48 to 0.57 mol%), Mg (pyrope component from 0.005 to 0.02 mol%) and Fe (almandine component from 0.22 to 0.32). The decreasing Mn content (spessartine component from 0.17 to 0.15 mol%) from core to rim indicates growth during heating (e.g. Spear et al., 1990).

(iii) Carbonates

Carbonates (Figs. 2a, c and f, sample P12-005) contain amphibole, epidote, apatite (>4 mm), idiomorphic biotite and oxides as minor mineral phases. The carbonate shows mostly a coarse-grained inequigranular-interlobate texture that includes the other rock-forming minerals. Up to 1 cm-sized calcite grains exhibit straight twinning. Locally, the coarse-grained calcite exhibits a faint sectorial extinction suggesting that the texture actually seen grew over a fine-grained polygonal texture. Veins carbonates can form crystals up to 30 cm long exhibiting straight twinning.

Locally, between the mafic dykes and the gneisses, transitional rock types with metasomatic textures were observed (Fig. 3a). Careful field inspection reveals, from the mafic boudin to the gneiss, the presence of: (i) an epidote amphibolite cut by a network of feldspar veins (sample P14-005, Fig. 3b); (ii) a white mica-amphibole-epidote-feldspar schist with white mica, amphibole and epidote forming a mineralogical layering (sample P14-004, Fig. 3c) and (iii) a feldspar-chlorite-white mica-amphibole-epidote schist with a protomylonitic foliation defined by chlorite, white mica and amphibole (sample P14-003).

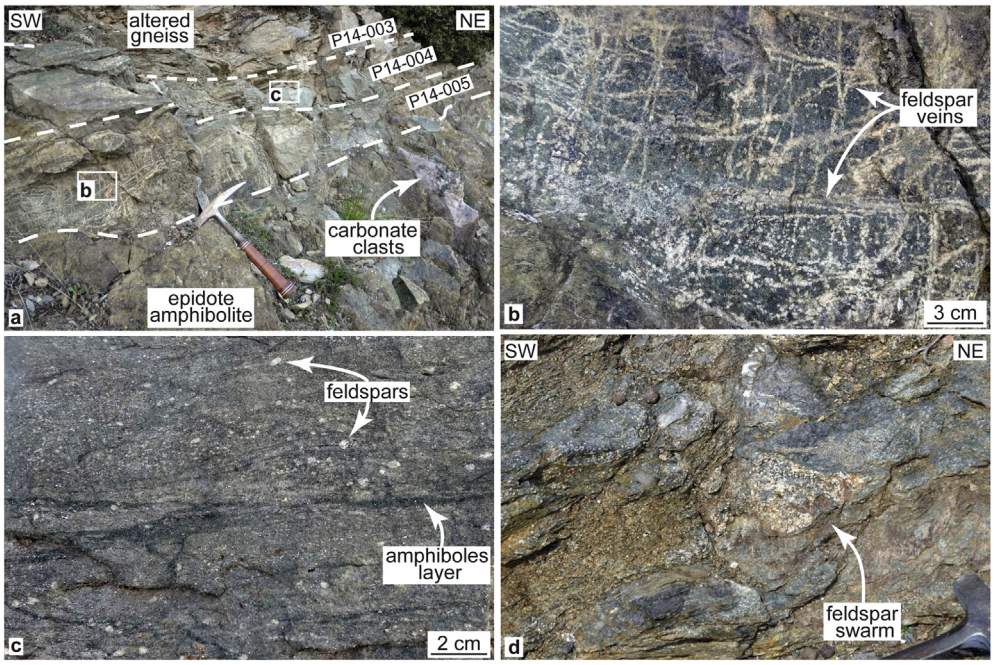

Fig. 3. Textural aspects of mafic rocks, country rock and fenites. (a) Transition zone between mafic-carbonatitic boudin and felsic country rock with sampling locations P14-003, P14-004 and P14-005 (frame b = subFig. 3b, frame c = subFig. 3c). (b) Epidote amphibolite cut by a network of feldspar veins (sample P14-005). (c) White mica-amphibolite-epidote-feldspar schist with an amphiboles layer (sample P14-004). (d) Feldspar swarm in the gneissic-schistose country rock resulted from channelized alkaline fluids. The alkali (Na and K) of the micas and feldspars were released during the crystallisation of the carbonatitic melts.

A detailed structural and petrographic account of the Pelagonian basement, which consists of metagranitoids with minor amphibolites and migmatites, is given in Schenker et al. (2014). Within approximately 100 m around the carbonate-amphibolite-epidotite association (Fig. 1), the country rocks show a large range of textures, from gneissic to schistose, depending on the mica content. The mineral assemblage comprises plagioclase, chlorite, white mica and quartz with local enrichments in plagioclase, paragonite, green amphibole and occasionally garnet and depletion of quartz. Rare idiomorphic feldspar and elongated mafic enclaves in the gneisses point to a granitoid protolith. Two types of schist were identified: (i) garnet-plagioclase-white mica-paragonite-chlorite schist and (ii) amphibole-chlorite-feldspar schist. The transition between gneisses and schists is usually gradual over 10–50 cm. In some schistose-gneissic rocks, feldspars form elliptic swarms (Fig. 3d). Such swarms, the white mica-paragonite layer within the amphibolite (Fig. 2e) and the white mica-amphibole-feldspar-rich layers (samples P14-003, P14-004 and P14-005) topping the dikes (Fig. 3a) are interpreted as the product of channelized alkaline fluids forming fenites. The schists represent either metasomatic rocks (e.g. metafenites) or metasediments. A single 20 cm leucocratic dike cuts the chemical layering of the fenites and refracts the main foliation attesting to a post-fenitization, pre-foliation intrusion.

About six (6) km east of the described amphibolite-epidotite-carbonate association, the gneissic basement is intruded by an andesitic dyke that displays a holocrystalline-porphyritic texture typical of subvolcanic intrusions. It is dated at 279 ± 8 Ma (sample 10-079, Schenker et al., 2014) and its alkaline geochemical signature will be re-interpreted in the light of the rocks described in this study.

4. Whole-rock and single-crystal geochemistry

Major- and trace-element abundances were measured at ETH Zurich using XRF and LA-ICP-MS techniques (see Appendix A). The mafic rocks (P12-004, P12-031, P12-033, 10-079), the carbonate (P12-005 = 0.038 wt%) and fenite sample P14-005 have all low alkali content ($Na_2O + K_2O$) and plot in the tholeiitic/subalkaline field in the TAS diagram (Fig. 4c). By contrast, fenite samples P14-003 and P14-004 are enriched in alkalis and fall in the field of the alkaline series in the above diagram. It should be noted, however, that the alkalis are mobile during metamorphism. On the other hand, the Nb/Y vs. Zr/TiO_2 diagram (Winchester and Floyd, 1977) is more efficient to discriminate between sub-alkaline and alkaline mafic rocks in metamorphic terrains because its construction was based on immobile elements (Pearce, 1996). In this diagram, mafic rocks P12-004 and P12-033 plot in the alkaline basalt, P12-031 in the sub-alkaline basalt, 10-079, P14-003 and P14-004 in the andesite and P14-005 in the trachy-andesite fields (Fig. 4d).

Chondrite-normalized REE profiles (Fig. 5a; subscript n denotes normalized values) of amphibolite P12-004, epidotite P12-033, andesitic dyke 10-079 and fenites P14-003, P14-004 and P14-005 show a gradual depletion from the LREE (La_n ~200–400) to the HREE (Lu_n ~15). Such concentrations and trends are diagnostic of alkaline rocks (e.g. Kampunzu and Mohr, 1991). Amphibolite P12-031 has a similar trend but at much lower concentrations. Calcite and apatite (P12-005, P12-005C, P12-035 and P12-031P) display REE_n profiles with antithetic trends compared to those of amphibolite, epidotite and the fenites, with low $LREE_n$ concentrations (La_n ~0.1) and $HREE_n$ enrichment (Lu_n ~30). Compared to average carbonatite, calcite and apatite are very depleted in $LREE_n$ but similar in $HREE_n$ concentrations (Ho_n to Lu_n, Fig. 5a). The observed Sm_n anomaly in apatite corresponds to deepening of the slope between Nd_n and Sm_n in the REE_n pattern of the amphibolite and epidotite (Fig. 5a). Such antithetic trends were also found between calcite phenocrysts and carbonatites from Spitskop, South Africa (Ionov and Harmer, 2002) and Brava Island, Cape Verde (Weidendorfer et al., 2016). According to the latter authors, carbonates from carbonatites with such LREE-depleted patterns could result from fluid-assisted carbonate recrystallization, linked either to fluid saturation in the final stage of crystallization or to an overprint by metasomatic fluids during fenitization. Importantly also, the recent experimental study of Song et al. (2016) on REE partitioning between hydrous fluids and carbonatitic melts at 700–800 °C and 0.1–0.2 GPa has shown the strong preference of REE to the melt (fluid–melt D values of individual REE vary from 0.02 to 0.15 with $D_{Lu}^{f/m}$ being larger than $D_{La}^{f/m}$ by a factor of 1.1–2), further suggesting that the REE-poor calcites may have precipitated from late-stage hydrous fluids in equilibrium with a carbonatitic melt. Such carbonate rocks (that form a continuum with primary magmatic carbonates and are

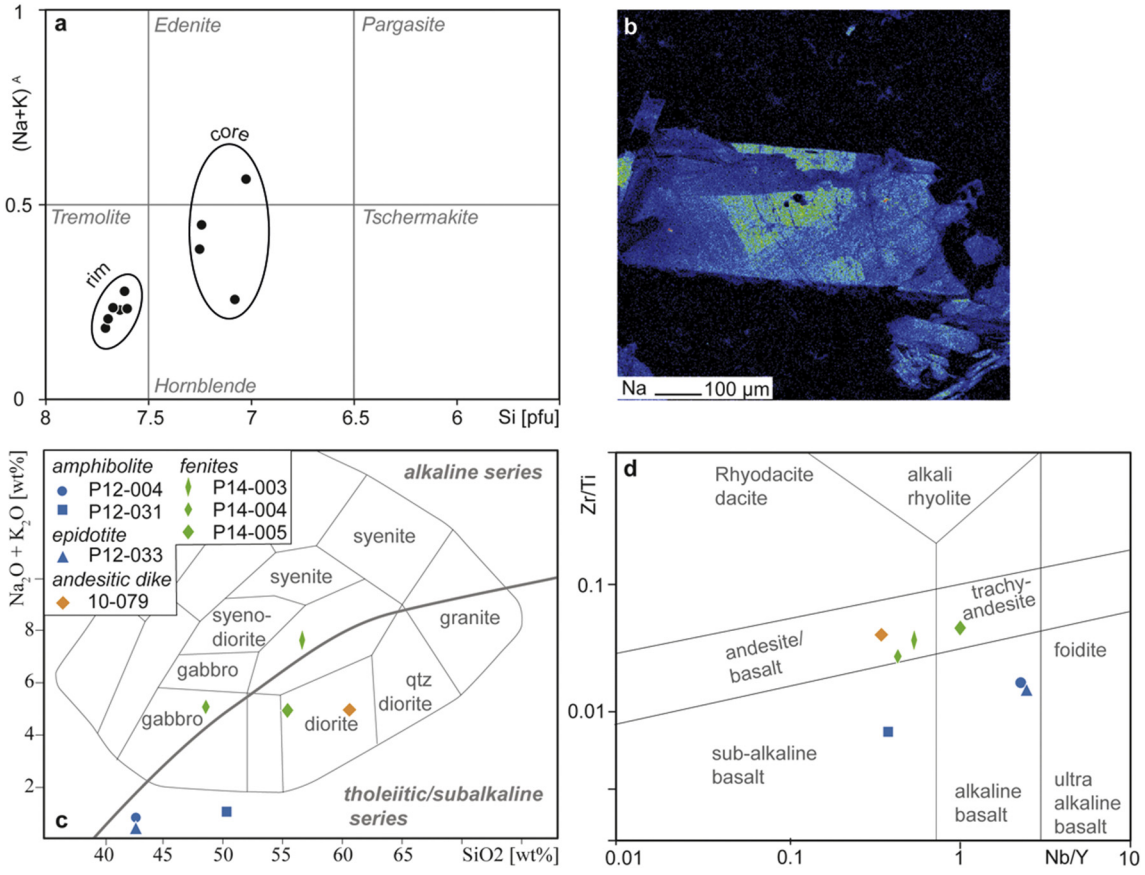

Fig. 4. (a) Classification of amphiboles after Deer et al. (1992) separating rims and cores. (b) Na-elemental map of an amphibole. Cool colours represent low concentration; warm colours high concentration, black minimum concentration. (c) TAS plot (Wilson, 1989). (d) Nb/Y vs. Zr/TiO2 plot (Winchester and Floyd, 1977). This diagram originally designed for volcanic rocks is commonly used to discriminate between sub-alkaline and alkaline mafic rocks in metamorphic terrains (Pearce, 1996), since the discriminating elements are not mobilized by metamorphism.

associated with sodic peralkaline syenites) resemble the carbonatite group termed "carbothermal residua" by Mitchell (2005). Similarly to the calcites discussed above, fluorapatites exhibiting a depletion in $LREE_n$ with respect to $HREE_n$ were observed in late-stage/hydrothermal carbonatites (Chakhmouradian et al., 2017). Apatite preferentially incorporates the middle REE (including Sm) during fractionation from a carbonatitic melt (Klemme and Dalpé, 2003). This could explain the positive anomaly of Sm_n and Eu_n in the apatites. Moreover, diffusion experiments on trace elements between immiscible carbonatitic and silicate melts have shown that enrichment of the carbonate liquid in REE occurs at P > 0.6 GPa (Hamilton et al., 1989). It is therefore possible that the overall low REE abundances and the $LREE_n$-depleted pattern in the Pelagonian carbonates can be due to late-stage liquid immiscibility and crystallization of a silicate and a carbonate at P < 0.6 GPa.

MORB-normalized multi-element profiles for the rocks under discussion are depicted in Fig. 5b. Reference to this figure shows an enrichment in $LILE_n$ and Th_n for the amphibolites, the epidotites, the andesitic dyke and the fenites. Barium is particularly concentrated in fenites P14-003 and P14-004 reaching values as high as ca. 0.3 wt%. Amphibolite P12-004 and epidotite P12-033 show high Nb_n and Ta_n values, typical of within-plate basalts. Elemental concentrations then decrease gradually from La_n to Yb_n. This negative trend coupled with low Y_n and $HREE_n$ values suggest that samples P12-004, P12-033 and 10-079 were sourced from garnet-bearing peridotite (Kostopoulos and James, 1992). However, andesitic dyke 10-079, amphibolite P12-031 and fenites P14-003, P14-004 and P14-005 show a negative Nb_n-Ta_n anomaly. The calcite crystal shows a U-shaped trace element pattern with an enrichment in Ba_n. Comparable, low-concentration, trends were found in late-stage Cape Verde carbonatites (Weidendorfer et al., 2016).

The geochemical signals described above (Fig. 5a and b) are compatible with late-stage carbonatites that evolved from fractionation and subsequent melt immiscibility (Weidendorfer et al., 2016). It is commonly argued that the primary melts are silica-dominated and exsolved their carbonate components late within the shallow lithosphere (e.g. Tappe et al., 2017). We suggest that the alkalis and LREE liberated from the carbonate rock portions during late, fluid-assisted, recrystallization (Weidendorfer et al., 2016) and/or during later metamorphism were taken up by the fenites. Fenites differ from the carbonate-mafic association by lower Nb-Ta and higher Rb-Ba concentrations.

5. $\delta^{13}C$ and $\delta^{18}O$ on carbonates and $\delta^{18}O$ on zircons

Powders of six carbonate samples from different hosts and textural positions were analysed for carbon and oxygen isotopes using a ThermoFisher GasBench at ETH Zurich. These are: calcite crystal P12-005 from the carbonate dyke shown in Figs. 1 and 6a; interstitial carbonates from amphibolite P12-004 (Fig. 2a) and epidotite P12-033; carbonate P12-034 in a vein with syntaxial growth of amphiboles (Fig. 6b); white carbonate vein P13-100 cutting mafic rocks and the main foliation in the country rock and marble 09-014 covering the Pelagonian basement (Fig. 1b). The marble sample shows $\delta^{13}C$ values from 2.42 to 2.45 (‰ vs. VPDB) and $\delta^{18}O$ values from 28.09 to 28.13 (‰ vs. VSMOW), typical of meta-sedimentary carbonates. Values of $\delta^{13}C$ from 1.77 to 1.81 and $\delta^{18}O$ from 23.11 to 23.07 were obtained for the late carbonate vein (P13-100), reflecting crustal fluids. In the mafic-related carbonate, $\delta^{13}C$ (−5.18 to −5.56) and $\delta^{18}O$ (10.68 to 11.59) (Fig. 6c, d) plot in the range of the Oka carbonatites (Canada, Deines, 1967), close to values of carbonatites included in the siliceous intrusion (Fig. 6d). The calcite

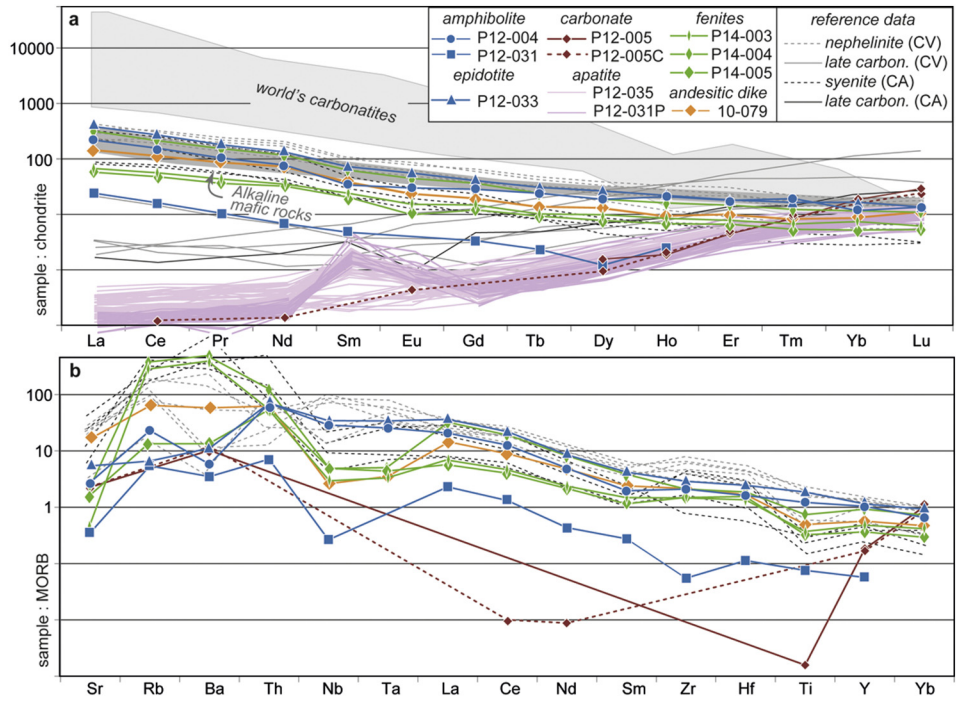

Fig. 5. (a) Chondrite-normalized (Sun and McDonough, 1989) REE and (b) MORB-normalized (Sun and McDonough, 1989) trace-element diagrams of the rock types forming the carbonate-mafic rocks lens, of the fenites and of andesitic dyke 10-079 (Schenker et al., 2014). Average values of carbonatites and alkaline mafic rocks from Woolley and Kempe (1989) and Kampunzu and Mohr (1991), respectively. Data of oceanic (Cape Verde, CV) and continental (Central Anatolia, CA) late-stage carbonatites with associated rocks from Weidendorfer et al. (2016) and Cooper et al. (2011), respectively. Apatite P12-035 is in textural contact with calcite and apatite P12-031P with amphibole. P12-005C has been measured directly on the calcite crystal.

crystal from the carbonate dyke yielded average values of -5.45 ± 0.03 for $\delta^{13}C$ and 10.81 ± 0.25 for $\delta^{18}O$ whereas the interstitial carbonates yielded average values of 5.47 ± 0.10 for $\delta^{13}C$ and 11.08 ± 0.21 for $\delta^{18}O$.

Carbon ($\delta^{13}C$) and oxygen ($\delta^{18}O$) isotopic compositions similar to those described above are observed in skarn/contact metamorphic carbonates due to magmatic or meteoric fluid infiltration (Fig. 6c, e.g.

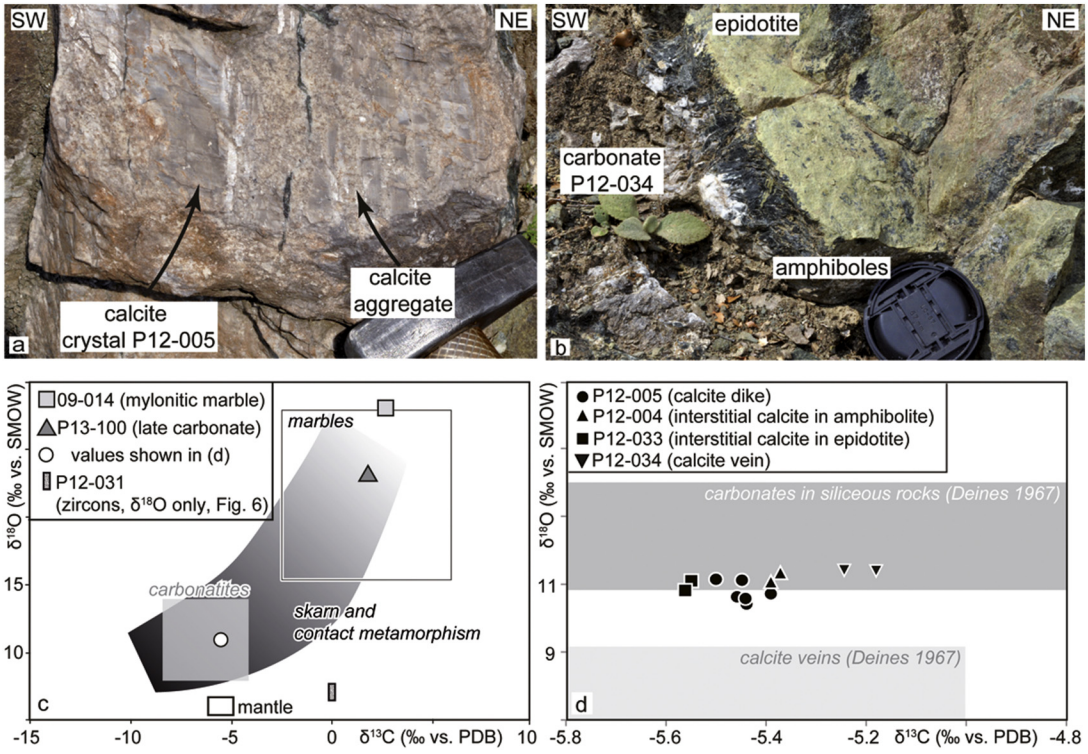

Fig. 6. Field aspects of analysed calcite ((a) and (b)) and analysed O and C isotopes on carbonates in different rock types and textures ((c) and (d)). Boxes show typical values for marbles (Sharp, 2007), skarn and contact metamorphic carbonates (Baumgartner and Valley, 2001) and carbonatite (Deines, 1967). The C mantle values are from peridotite diamonds (Deines, 1980) and O mantle values from the Oka terrain (Harmon and Hoefs, 1995).

Baumgartner and Valley, 2001). In such an environment, the $\delta^{13}C$ and $\delta^{18}O$ isotopic values of the country-rock carbonate decrease to carbonatitic values with proximity to the intrusion (shift from 0 to −6 ‰ for $\delta^{13}C$ and from 22 to 10 ‰ for $\delta^{18}O$ within 10 m distance from a 0.5–1 m thick gabbro dyke of the Adamello intrusion; Baumgartner, 1986; Baumgartner and Valley, 2001), whereas the heterogeneity of the values increases (e.g. variability of ~10‰ for $\delta^{18}O$ in the southern Alta contact aureole, Cook et al., 1997). By contrast, the calcite crystals from the carbonate dykes we presented here showed minor variability in $\delta^{13}C$ and $\delta^{18}O$ values in all textural contexts demonstrating that there was minimal lateral variation and internal fractionation during the emplacement process. Furthermore, the absence of (i) a metamorphic aureole in the country rock and (ii) of siliceous dykes in the mylonitic marble that could have generated skarn metasomatism (Fig. 1) suggest that the obtained carbonatitic isotope values are not related to skarn-related fluids. On the contrary, the structural and textural observations attesting that mafic and carbonate rock portions are included within boudinaged dykes suggest that the negative $\delta^{13}C$ and probably also the $\delta^{18}O$ signatures were advected from an already negative in $\delta^{13}C$ and low in $\delta^{18}O$ reservoir: the mantle.

The $\delta^{18}O$ composition of zircons from the carbonate-bearing amphibolite P12-031 were analysed at the SwissSIMS in Lausanne. The CL images (Fig. 7a and Appendix B) show a morphologically homogeneous population of prismatic, elongated and euhedral crystals with a pale zoning truncating a dark core with patchy and oscillatory zoning characteristic of magmatic zircons (Corfu et al., 2003). The zircon grains contain carbonate inclusions. Five dark zircon cores yielded a mean $\delta^{18}O$ of 7.31 ± 0.20 (‰ vs. VSMOW), less negative with respect to the mean $\delta^{18}O$ of 6.90 ± 0.12 of the 12 pale zircon domains. The $\delta^{18}O$ values of the zircons are consistent with a magmatic $\delta^{18}O$ zircon composition (e.g. Valley, 2003). Later thermal re-equilibration most likely produced the more negative $\delta^{18}O$ values of the pale rims. Intercrystalline stable isotope diffusion can locally lower the $\delta^{18}O$ values of the slow diffuser mineral (zircon) at conditions below its closing temperature during a low-temperature event while the fast diffusing mineral is dominant (calcite, Eiler et al., 1992). This magmatic $\delta^{18}O$ composition above the typical mantle values (Fig. 7b), the morphology of zircons with internal magmatic zoning and carbonate inclusions suggest together that the zircons crystallized from a carbonatitic melt and are not clasts from the mantle.

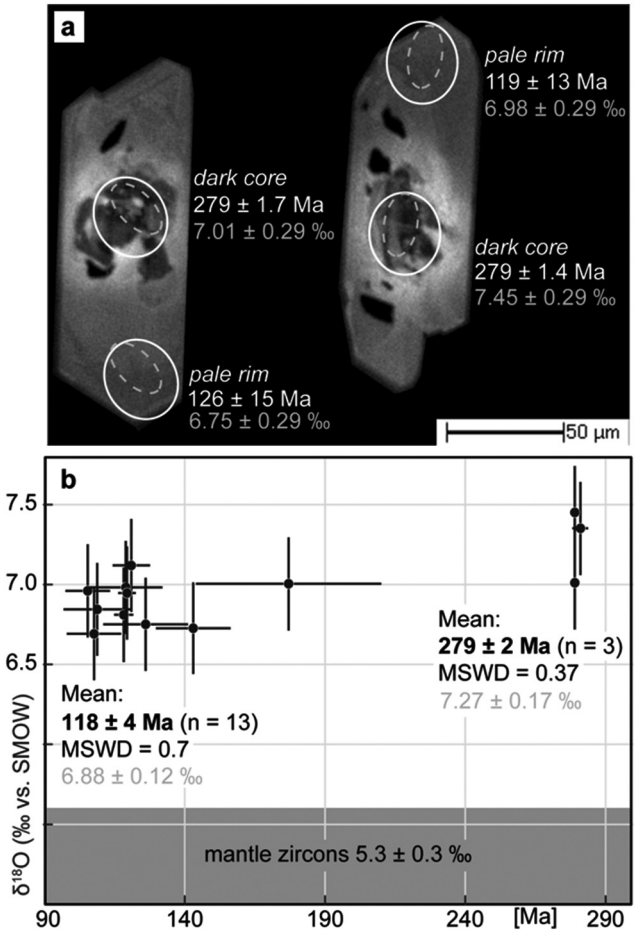

Fig. 7. a) Cathodoluminescence images of zircons with spot analyses ages and $\delta^{18}O$ values (‰ vs. VSMOW) from amphibolite sample P12-031. b) $\delta^{18}O$ vs. age of single analytical spots in zircons. Mean ages from Tera-Wasserburg (Permian magmatic core) and weighted mean age (Cretaceous metamorphic rims) diagrams from SHRIMP II analyses (Appendix B). The Concordia ages have errors at 95% confidence intervals. MSWD is the sum of squares of weighted residuals divided by the degrees of freedom of the calculation. Mean O isotopic concentration for mantle zircons from Valley et al. (1998).

6. U–Pb geochronology on zircons

The same zircons from sample P12-031 were dated with a SHRIMP II at VSEGEI, Saint-Petersburg, Russian Federation. Three inclusion-free, dark zircon cores yielded concordant U-Pb ages at 279 ± 2 Ma and 13 pale zircon domains yielded mean ages of 118 ± 4 Ma (Fig. 7b). Thorium/uranium (Th/U) ratios of all measurements vary in the dark cores between 0.09 and 0.53 and in the pale domains between 0.002 and 0.016. The latter low Th/U values are generally indicative of metamorphic zircon domains (e.g. Teipel et al., 2004), suggesting that the core ages record Permian intrusion and the rims Cretaceous metamorphism already corroborated in the area by U–Pb, Rb–Sr, and Ar–Ar dating (Lips et al., 1998; Schenker et al., 2014; Schermer et al., 1990; Yarwood and Dixon, 1977).

7. Sr and Nd isotopes

Sr and Nd isotopes on calcitic vein P12-005, an apatite of Fig. 2d, epidotite P12-033, amphibolite P12-004 and andesitic dyke 10-079 were measured with total dissolution thermal ionization mass spectrometry at ETH Zurich. The $^{87}Sr/^{86}Sr$ ratio ranges from 0.704202 to 0.710574, i.e. from more mantle to more crustal values. Nonetheless, the Rb-Sr isotopic signal of most Pelagonia basement rocks was modified during the late Lower Cretaceous metamorphic episode. Strontium with a high $^{87}Sr/^{86}Sr$ ratio (0.737409), was mobilized from Neoproterozoic rocks resting tectonostratigraphically below the studied outcrops during metamorphism, and strongly affected (increased) the $^{87}Sr/^{86}Sr$ ratio of most younger orthogneisses (Schenker et al., 2014). Especially in carbonate-bearing rocks, the mobility of Sr is expected to be more pronounced since Sr diffusion in calcite is 2–3 orders of magnitude faster than it is in feldspars (Cherniak, 1997). As a consequence, the Rb-Sr isotopic signal is neither used for melt provenance analysis nor for geochronology. As an exception, the less metasomatized andesitic dyke has preserved a more mantle-like $^{87}Sr/^{86}Sr$ ratio at 0.704202.

Neodymium isotope ratios ($^{143}Nd/^{144}Nd$) vary between 0.512411 and 0.512665 reflecting typical mantle values (Fig. 8a). Concentrations of Nd isotopes in the carbonate sample were below the detection limits. No isochron could be drawn between the cogenetic amphibolites, epidotites and apatites (Fig. 8a), suggesting that the Sm–Nd isotopic system was either in disequilibrium during primary emplacement or has been partially reopened during metamorphic overprint. In addition, andesitic dyke 10-079 does not conform to an isochron with the mafic-carbonatic rocks (Fig. 8a).

Epsilon Nd values ($\varepsilon_{Nd(t)}$; DePaolo and Wasserburg, 1976) of amphibolites, epidotites, apatites and andesite calculated at the time of the intrusion (279 Ma) range between −1.33 and 4, and fall in the global carbonatite field (Fig. 8b). Pelagonian magmatism younger than ca. 310 Ma (Fig. 8b; Schenker et al., 2014) shows a shift in ε_{Nd} values from typical crustal ($\varepsilon_{Nd(301\ Ma)} = -7.33$) to primitive mantle levels ($\varepsilon_{Nd(279\ Ma)} = -1.33$, ~0 and 4 in the andesitic dyke, mafic rocks and

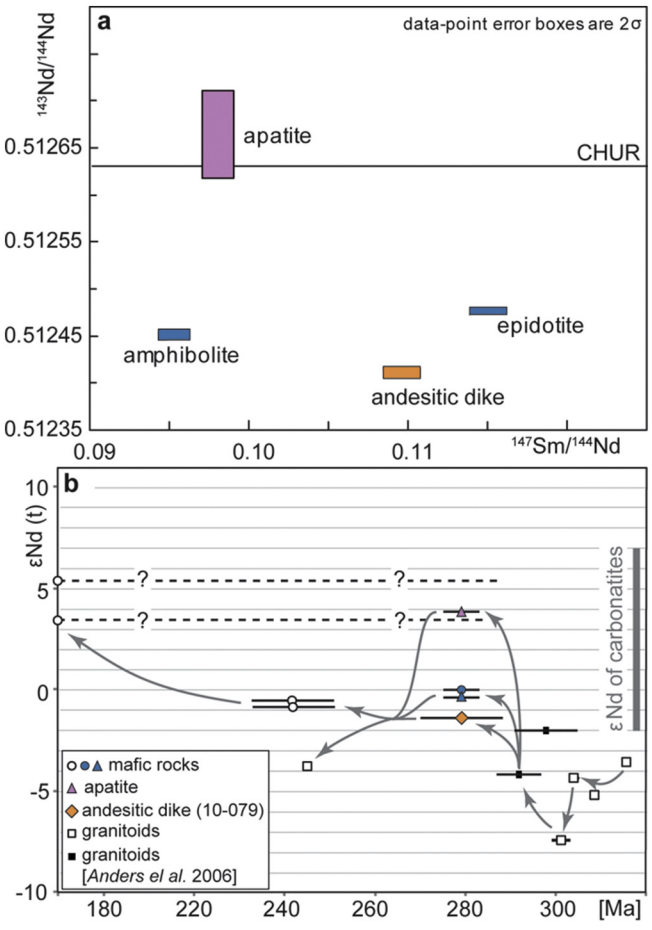

Fig. 8. Nd isotope plots of the constituent rocks of the carbonatitic and andesitic dykes. (a) $^{143}Nd/^{144}Nd$ and $^{147}Sm/^{144}Nd$ rations. (b) εNd evolution of the magmatism of the Pelagonia zone according to Schenker et al. (2014). εNd(t) calculated for the age t of the intrusions. εNd(t) compared with carbonatite values worldwide (Bell and Blenkinsop, 1989).

apatite respectively). Thereafter, in the Lower Triassic, ε_{Nd} values decreased in both mafic and felsic rocks, probably due to crustal contamination, to rise again to mantle values in the Jurassic. This 300-to-175 Ma evolution of ε_{Nd} in Pelagonian magmatism is attributed to a continuous melt contribution from the rising asthenosphere that destabilized the continental lithosphere in the Permian, promoted initiation of continental rifting in the Triassic and led to the development of an ocean in the Jurassic. The fluctuations in ε_{Nd} towards negative values are interpreted as crustal contamination (migmatitic melts in response to asthenospheric upwelling; see Schenker et al., 2012).

8. Discussion

8.1. Real carbonatites?

The coeval intrusion of distinct carbonatitic and mafic liquids into the crystalline basement of the Pelagonian Zone is demonstrated by field and textural relationships between the carbonatic and the mafic rock portions and gneissic country rocks. These observations invalidate other scenarios such as a skarn-type metasomatism or carbonate-bearing magmatic xenoliths. Carbonatites are generally characterized by their typical geochemical imprint consisting of (i) a spatio-temporal association with alkaline suites, (ii) fenitization of the country rocks and (iii) high concentrations of LREE, Sr, Ba, and P. The newly discovered carbonatitic dykes are indeed coeval with other silicate rocks with an alkaline geochemical signature (andesite 10-079) intruded during the early Permian in the Pelagonian basement. In addition, the country rock around the carbonate-mafic dykes was impregnated by channelized alkaline fluids forming fenites that attest to the alkalinity of the parental melt. Fenites forming at shallow depth due to the high reactivity of carbonatitic liquids with their wall-rocks are probably one of the most important features in defining carbonatites (Le Bas, 1989). In the Pelagonian case, the usually high concentrations of LREE and Sr were not observed in the carbonate or the mafic rock portions. High concentrations of Ba (0.3 wt%) in the fenites are probably taken up from the alkaline-carbonatitic fluid. Phosphorus is incorporated in large apatite crystals implying high bulk P concentrations. However, because of the size of the apatite crystals (up to 10 cm), whole-rock P concentrations are difficult to estimate. Regarding the low LREE concentrations, it is worth mentioning that not all carbonatitic-alkaline complexes have unusually high REE concentrations; moreover, REE concentrations can change within individual carbonatitic-alkaline complexes. In this view, a comparison with late-stage carbonatites from Cape Verde (Weidendorfer et al., 2016) and Central Anatolia (Cooper et al., 2011) suggests that the antipathetic REE_n trends between carbonatic and alkaline mafic rock portions of the Pelagonian dyke result from late-stage liquid immiscibility and crystallization. The alkaline parental melt of these liquids may have already been depleted in REE due to previous fractional crystallization (Xu et al., 2010; Chakhmouradian et al., 2016).

The Pelagonian carbonatitic dykes have been metamorphosed at greenschist-facies conditions as manifested by the tremolitic rims on Na-rich amphibole cores in the mafic rocks and by the chlorites in the fenites. The amphibole cores may preserve a carbonatitic composition comparable to the Ca-amphiboles of the Pinghe carbonatites and the Al-poor Ca-Na amphibole of the Afrikanda carbonatites (Reguir et al., 2012). The metamorphism further complicated an already complex intrusive scenario of immiscible carbonate and silicate melts and metasomatism. It is indeed difficult to quantify the effect of metamorphism on the chemical signature of these late stage-carbonatites, especially with regard to the isotopes used in magmatic provenance analysis.

The absence of carbonate in the country rocks and the minor variation in the $\delta^{13}C$ and $\delta^{18}O$ composition of carbonates from different structural and textural positions both suggest that the carbonate-silicate association acted as a closed system, at least for these elements. At the grain scale, metamorphism brought about local resetting of the zircon O and U–Pb isotopic systems, thus allowing the estimation of the timing of the greenschist metamorphic overprint. This comes into contrast with the experimentally-determined high closure temperatures (>700 °C) for both isotopic systems in zircon (e.g. Watson and Cherniak, 1997). Interestingly, the U–Pb system of zircons in metacarbonatites from the southern Cordillera of British Columbia appears to have reopened below its closure temperature at amphibolite-facies metamorphic conditions between 540° and 730 °C (Millonig et al., 2013). Hence, the U–Pb isotopic system in zircons seems to be sensitive to carbonatitic, alkali- and/or F-rich fluids (Keppler, 1993). Fenites and fluorapatites confirm the presence of alkalis and F in the Pelagonian carbonatites.

Strontium isotopes were mobile during the Cretaceous metamorphism. Within the Pelagonian basement, high $^{87}Sr/^{86}Sr$ ratios (0.737409) mobilized from Archean rocks elevated the $^{87}Sr/^{86}Sr$ ratio of carbonatites, mafic rocks and metagranitoids to more crustal values therefore, these isotopes are not used for provenance analysis (Schenker et al., 2014). Certain rocks apparently not affected by metasomatism, for example the andesitic dyke, have retained primitive $^{87}Sr/^{86}Sr$ ratio values (e.g. 0.704202 for the andesite).

8.2. Transtensional carbonatites

The primitive ε_{Nd}, $\delta^{13}C$ and $\delta^{18}O$ values of the Pelagonian late-stage carbonatites (Fig. 9) strongly indicate that they originated either from a depleted or a deep mantle source in rift settings and not from a mantle source in a subduction-zone environment (see also Vladykin, 2016). This conclusion is in agreement with an increase of mantle-related,

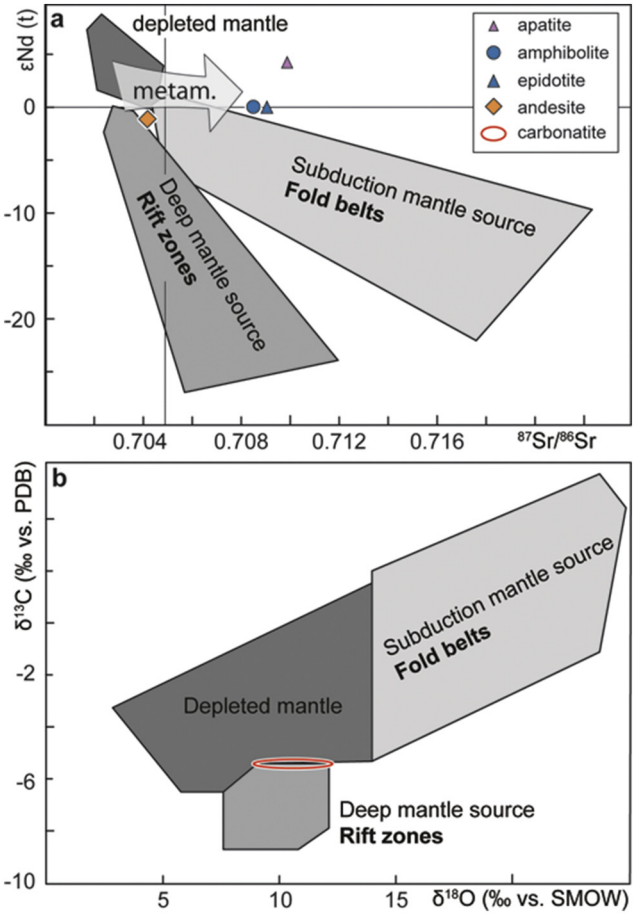

Fig. 9. (a) Sr-Nd and (b) C-O discrimination diagrams for alkaline carbonatite complexes according to Vladykin (2016). The Pelagonian alkaline carbonatite rocks have an εNd, $\delta^{13}C$ and $\delta^{18}O$ values that plot between the fields of the depleted and deep mantle source in rift settings. Sr isotopes are not considered for magmatic provenance analysis since they were altered during metamorphism by mobile high $^{87}Sr/^{86}Sr$ ratios (0.737409) from Archean rocks deeper within the Pelagonian basement (Schenker et al., 2014).

primitive melts in the Pelagonian magmatism from 300 to 175 Ma and the absence of Late Carboniferous accretionary complexes, blueschists or eclogites, and deep forearc basins in the Balkans. We suggest that these alkaline-carbonatitic rocks intruded within transtensional segments of the recognized, wide intra-Pangea dextral wrench system (Arthaud and Matte, 1977; Muttoni et al., 2009).

9. Conclusions

C- and O-mantle signatures in carbonates associated with alkali amphibolites and metafenites support the carbonatitic protolith of these metamorphic rocks in the Pelagonian Zone in NW Greece. Mantle carbonates ($\delta^{13}C$ of −5 ‰ vs. VPDB) and alkali basaltic liquids (with high Nb_n-Ta_n and ε_{Nd} values) were intruding contemporaneously as documented by carbonates truncating and being incorporated in both amphibolites and epidotites within boudinaged dykes. The REE_n antithetic trends between mafic rocks and carbonates/apatites further witness their complementarity during late-magmatic liquid immiscibility and fluid-assisted recrystallization. Low REE_n and relatively high Ba_n concentrations are found in extremely differentiated carbonatites (Weidendorfer et al., 2016). Channelized alkaline fluids penetrated into the country rock forming fenites and attesting to the alkalinity of the parental melt. The intrusion age is dated by concordant magmatic zircon cores at 279 ± 2 Ma.

The gradual increase of ε_{Nd} in the studied magmatic rocks through time (from 300 to 175 Ma) reflects an increase of mantle-derived magmas sourced from the mantle upwelled below the Pelagonian zone. The 279 ± 2 Ma-old alkaline-carbonatitic melts intruded within transcurrent segments of a wide intra-Pangaea dextral transform (the Pangaea B model, Arthaud and Matte, 1977; Muttoni et al., 2009). These melts suggest preconditioning of the sub-Pelagonian lithosphere for rifting since the Lower Permian. The possible role of subduction of the Palaeotethys Ocean beneath Laurussia (e.g. Candan et al., 2016; Stamfli and Kozur, 2006) in the genesis of the Pelagonian carbonatites is unclear. Metamorphic zircon ages at 118 ± 4 Ma date the greenschist-facies thermal event during collision of the Pelagonian Zone with the Eurasian margin (Schenker et al., 2014).

Acknowledgement

This work was supported by ETH research grant ETH-09 09-3 and by the University of Lausanne. We thank Stefano Bernasconi, Marcel Guillong, Alexander Larionov, Sergey A. Sergeev and Albrecht von Quadt for analytical support and Andrea Galli for constructive discussions and analytical help. We thank Jindrich Kynický, Nikolay Vladykin and an anonymous reviewer for their thorough reviews, their inputs and their criticism, which helped clarifying concepts and interpretations.

Appendix A. Methods

XRF analysis

Whole-rock XRF analyses were performed on fused disks using a Panalytical Axios wavelength dispersive spectrometer (WDXRF, 2.4 KV) at ETH Zurich. Samples were ground to fine powder in an agate mill and mixed with lithium tetraborate at 1:5 ratio and molten to homogenous glass disks. The spectrometer is set up for 12 major and minor elements (SiO_2, TiO_2, Fe_2O_3, MnO, MgO, CaO, Na_2O, K_2O, P_2O_3, Cr_2O_3, and NiO) and 19 trace elements (Rb, Ba, Sr, Nb, Zr, Hf, Y, Ga, Zn, Cu, Co, V, Sc, La, Ce, Nd, Pb, Th, and U).

WDS the electron microprobe JEOL-8200

Mineral compositions were measured using WDS the electron microprobe JEOL-8200 (5 spectrometers) at ETH Zurich. Operating conditions for spot analyses were 15 kV accelerating voltage, 20 nA sample current, 40 s peak and 20 s background counting time and beam size of <5 μm. Natural and synthetic standards were used for standardisation. Minerals were analysed for SiO_2, TiO_2, Cr_2O_3, Al_2O_3, FeO, MnO, MgO, CaO, Na_2O, and K_2O. Amphibole data were recalculated from analyses in weight percent according to Dale et al. (2005).

LA-ICP-MS

Trace elements were measured at ETHZ with Laser Ablation-Inductively Coupled Plasma-Mass Spectrometry (LA-ICP-MS) on fused XRF pills calibrated without matrix-matched standards (Günther et al., 2001). Measuring time per spot was about 1 min and used energy density was 15 J/cm^2 at a frequency of 12 Hz. For each pill we analyzed 3 spots (90–120 μm diameter). CaO and SiO_2 values of XRF measurement were used as internal standards and calibrated against the NIST 610 for the data correction with SILLS. The expected measuring error is ~2% close to detection limit and even smaller in higher concentrations.

ThermoFisher GasBench

The isotopic composition of carbonate was measured according to the method described in detail in Breitenbach and Bernasconi (2011). Approximately 100–200 μg of powder were filled in 12 ml Exetainers (Labco, High Wycombe, UK) and flushed with pure

Helium. The samples were reacted with 3–5 drops of 100% phosphoric acid at 70 °C with a ThermoFisher GasBench device connected to a ThermoFisher Delta V mass spectrometer. The average long term reproducibility of the measurements based on replicated standards was ±0.05‰ for $\delta^{13}C$ and ±0.06‰ for $\delta^{18}O$. The instrument is calibrated with the international standards NBS19 ($\delta^{13}C = 1.95$ and $\delta^{18}O = -2.2$‰) and NBS18 ($\delta^{13}C = -5.01$ and $\delta^{18}O = -23.01$‰). The isotope values are reported in the conventional delta notation with respect to VPDB (Vienna Pee Dee Belemnite).

Sr/Nd chemistry

Samples were analysed for Sr and Nd isotopes on powdered bulk samples. Samples were dissolved in HF (3 mL) and HNO_3 (1 mL) for 5 days in Teflon beakers at 180 °C. This process was repeated after evaporation. Solutions were analyzed with thermal ionization mass spectrometry using a Triton plus multicollector spectrometer. Standards were National Bureau of Standards (NBS) 987 (0.710234 ± 4) for Sr and Nd_i (0.512100 ± 3) for Nd.

SHRIMP II

In situ U-Pb analyses on zircons were performed with a SHRIMP II in the Center of Isotopic Research (CIR) at VSEGEI, Saint-Petersburg. We applied a secondary electron multiplier in peak-jumping mode according to the procedure of Williams (1998) and Larionov et al., 2004. The primary O^{2-} beam was ca. 27 x 20 μm in size. The results have been post-processed with the SQUID v1.12 (Ludwig, 2005a) and ISOPLOT/Ex 3.22 (Ludwig, 2005b) softwares using the decay constants of Steiger and Jäger (1977). The ages were presented on Concordia (Wetherill, 1956) and Tera-Wasserburg (Tera and Wasserburg, 1972) diagrams. Uncertainties given for individual analyses (ratios and ages) are at the 1σ level; the uncertainties in calculated Concordia ages are reported at the 2σ level.

The pale zircon zonings were characterized by very low concentration of uranium (1–39 ppm) producing ages with large uncertainties. Because of the low concentrations, common Pb was corrected by assuming $^{206}Pb/^{238}U$-$^{207}Pb/^{235}U$ age concordance and not by using measured ^{204}Pb.

SIMS analytical conditions

The $^{18}O/^{16}O$ ratios on zircons were measured using a Cameca IMS 1280HR at the Institute of Earth Sciences of the University of Lausanne (Switzerland). We used a 10 kV Cs+ primary beam, a ~2 nA current, resulting in a ~10 μm beam size. The electron flood gun, with normal incidence, was used to compensate charges. ^{16}O and ^{18}O secondary ions, accelerated at 10 kV, were analyzed at 2400 mass resolving power and collected on faraday cups (10^{10} and ohms, respectively) in multi-collection mode. Faraday cups are calibrated in the beginning of the session, using the calibration routine. Mass calibration was performed at the beginning the session, which lasted less than 3 h. Each analysis takes less than 4 min, including pre-sputtering (30 s) and automated centering of secondary electrons. This setting allowed an average reproducibility of 0.3‰ (2 standard deviations (SD)) on a Temora zircon reference material (Black et al., 2004) and statistical internal error on a single measurement from 0.12 to 0.26‰ (2 standard error (SE)).

Appendix B. Supplementary data

Supplementary data to this article can be found online at https://doi.org/10.1016/j.lithos.2018.01.011.

References

Anders, B., Reischmann, T., Kostopoulos, D., Poller, U., 2006. The oldest rocks of Greece: first evidence for a Precambrian terrane within the Pelagonian Zone. Geological Magazine 143, 41–58.

Anders, B., Reischmann, T., Kostopoulos, D., 2007. Zircon geochronology of basement rocks from the Pelagonian Zone, Greece: constraints on the pre-Alpine evolution of the westernmost Internal Hellenides. International Journal of Earth Sciences 96, 639–661.

Arthaud, F., Matte, P., 1977. Late Paleozoic strike-slip faulting in southern Europe and northern Africa: result of a right-lateral shear zone between the Appalachians and the Urals. Geological Society of America Bulletin 88, 1305–1320.

Baumgartner, L.P., 1986. Petrologie und Geochemie stabiler Isotopen von zonierten metasomatischen Gesteinen der SW-Adamello Kontakt-Aureole Italien.

Baumgartner, L.P., Valley, J.W., 2001. Stable isotope transport and contact metamorphic fluid flow. Reviews in Mineralogy and Geochemistry 43, 415–467.

Bell, K., Blenkinsop, J., 1989. Neodymium and strontium isotope geochemistry of carbonatites. Carbonatites: Genesis and Evolution, pp. 278–300.

Black, L.P., Kamo, S.L., Allen, C.M., Davis, D.W., Aleinikoff, J.N., Valley, J.W., Mundil, R., Campbell, I.H., Korsch, R.J., Williams, I.S., 2004. Improved 206 Pb/238 U microprobe geochronology by the monitoring of a trace-element-related matrix effect; SHRIMP, ID–TIMS, ELA–ICP–MS and oxygen isotope documentation for a series of zircon standards. Chemical Geology 205, 115–140.

Breitenbach, S.F.M., Bernasconi, S.M., 2011. Carbon and oxygen isotope analysis of small carbonate samples (20 to 100 mμg) with a GasBench II preparation device. Rapid Communications in Mass Spectrometry 25, 1910–1914.

Brooker, R.A., Kjarsgaard, B.A., 2011. Silicate-carbonate liquid immiscibility and phase relations in the system SiO_2-Na_2O-Al2O_3-CaO-CO_2 at 0·1–2·5 GPa with applications to carbonatite genesis. Journal of Petrology 52, 1281–1305.

Candan, O., Akal, C., Koralay, O., Okay, A., Oberhänsli, R., Prelević, D., Mertz-Kraus, R., 2016. Carboniferous granites on the northern margin of Gondwana, Anatolide-Tauride block, Turkey–evidence for southward subduction of paleotethys. Tectonophysics 683, 349–366.

Chakhmouradian, A.R., Reguir, E.P., Couëslan, C., Yang, P., 2016. Calcite and dolomite in intrusive carbonatites. II. Trace-element Variations. Mineralogy and Petrology. 110, pp. 361–377.

Chakhmouradian, A.R., Reguir, E.P., Zaitsev, A.N., Couëslan, C., Xu, C., Kynický, J., Mumin, A.H., Yang, P., 2017. Apatite in carbonatitic rocks: compositional variation, zoning, element partitioning and petrogenetic significance. Lithos 274.

Chen, W., Simonetti, A., 2013. In-situ determination of major and trace elements in calcite and apatite, and U–Pb ages of apatite from the Oka carbonatite complex: insights into a complex crystallization history. Chemical Geology 353, 151–172.

Cherniak, D., 1997. An experimental study of strontium and lead diffusion in calcite, and implications for carbonate diagenesis and metamorphism. Geochimica et Cosmochimica Acta 61, 4173–4179.

Coltice, N., Simon, L., Lécuyer, C., 2004. Carbon isotope cycle and mantle structure. Geophysical Research Letters 31 (n/a-n/a).

Cook, S.J., Bowman, J.R., Forster, C.B., 1997. Contact metamorphism surrounding the Alta stock: finite element model simulation of heat-and 18O/16O mass-transport during prograde metamorphism. American Journal of Science 297.

Cooper, A.F., Boztuğ, D., Palin, J.M., Martin, C.E., Numata, M., 2011. Petrology and petrogenesis of carbonatitic rocks in syenites from central Anatolia, Turkey. Contributions to Mineralogy and Petrology 161, 811–828.

Corfu, F., Hanchar, J.M., Hoskin, P.W.O., Kinny, P., 2003. Atlas of zircon textures. Zircon 53, 469–500.

Cullers, R.L., Graf, J.L., 1984. Rare earth elements in igneous rocks of the continental crust: intermediate and silicic rocks-ore petrogenesis. Rare Earth Element Geochemistry. Elsevier, Amsterdam, pp. 275–308.

Dale, J., Powell, R., White, R.W., Elmer, F.L., Holland, T.J.B., 2005. A thermodynamic model for Ca-Na clinoamphiboles in Na_2O-CaO-FeO-MgO-Al_2O_3-SiO_2-H_2O-O for petrological calculations. Journal of Metamorphic Geology 23, 771–791.

Deer, W.A., Howie, R.A., Zussman, J., 1992. An Introduction to the Rock-Forming Minerals. Pearson Education, Harlow, England.

Deines, P., 1967. Stable Carbon and Oxygen Isotopes of Carbonatite Carbonates and Their Interpretation. The Pennsylvania State University, University Park.

Deines, P., 1980. The carbon isotopic composition of diamonds - relationship to diamond shape, color, occurrence and vapor composition. Geochimica et Cosmochimica Acta 44, 943–961.

Depaolo, D.J., Wasserburg, G.J., 1976. Inferences about magma sources and mantle structure from variations of 143Nd/144Nd. Geophysical Research Letters 3, 743–746.

Dyulgerov, M., Ovtcharova, M., Schaltegger, U., 2010. Unraveling the Time of Formation of Potassic-Alkaline Rocks in the Variscan Edifice in Stara Planina. ID-TIMS and LA-ICP-MS study. XIX CONGRESS OF THE CARPATHIAN-BALKAN GEOLOGICAL ASSOCIATION Thessaloniki, Abstract volume, Bulgaria, pp. 106–107.

Egorov, L.S., 1970. Carbonatites and ultrabasic-alkaline rocks of the Maimecha-Kotui region. N. Siberia. Lithos 3, 341–359.

Eiler, J.M., Baumgartner, L.P., Valley, J.W., 1992. Intercrystalline stable isotope diffusion: a fast grain boundary model. Contributions to Mineralogy and Petrology 112 (4), 543–555.

Falloon, T.J., Green, D.H., 1989. The solidus of carbonated, fertile peridotite. Earth and Planetary Science Letters 94, 364–370.

Freestone, I., Hamilton, D., 1980. The role of liquid immiscibility in the genesis of carbonatites—an experimental study. Contributions to Mineralogy and Petrology 73, 105–117.

Godfriaux, I., Ferriere, J., Schmitt, A., 1988. Le développement en contexte continental d'un métamorphisme HP/BT: les "schistes bleus" tertiaires Thessaliens. Bolletin of the Geological Society of Greece XX 175–192.
Günther, D., von Quadt, A., Wirz, R., Cousin, H., Dietrich, F.J., 2001. Elemental analyses using laser ablation-inductively coupled plasma-mass spectrometry (LA-ICP-MS) of geological samples fused with $Li_2B_4O_7$ and calibrated without matrix-matched standards. Mikrochim. Acta 136, 101–107.
Hamilton, D., Bedson, P., Esson, J., 1989. The behaviour of trace elements in the evolution of carbonatites. Carbonatites: Genesis and Evolution. Unwin Hyman, London, pp. 405–427.
Harmon, R.S., Hoefs, J., 1995. Oxygen-isotope heterogeneity of the mantle deduced from global O-18 systematics of basalts from different geotectonic settings. Contributions to Mineralogy and Petrology 120, 95–114.
Ionov, D., Harmer, R.E., 2002. Trace element distribution in calcite–dolomite carbonatites from Spitskop: inferences for differentiation of carbonatite magmas and the origin of carbonates in mantle xenoliths. Earth and Planetary Science Letters 198, 495–510.
Jacobshagen, V., Dürr, S., Kockel, F., Kopp, K.O., Kowalczyk, G., Berckhemer, H., Büttner, D., 1978. Structure and geodynamic evolution of the Aegean region. In: Cloos, H., Roeder, D., Schmidt, K. (Eds.), Alps, Appenines. Hellenides. E. Schweizerbart'sche Verlagsbuchhandlung, Stuttgart, pp. 537–564.
Jones, A.P., Genge, M., Carmody, L., 2013. Carbonate melts and carbonatites. Rev Mineral Geochem 75, 289–322.
Kampunzu, A.B., Mohr, P., 1991. Magmatic Evolution and Petrogenesis in the East African Rift System, Magmatism in Extensional Structural Settings. Springer, pp. 85–136.
Keppler, H., 1993. Influence of fluorine on the enrichment of high field strength trace elements in granitic rocks. Contributions to Mineralogy and Petrology 114, 479–488.
Kilias, A., Frisch, W., Avgerinas, A., Dunkl, I., Falalakis, G., Gawlick, H.J., 2010. Alpine architecture and kinematics of deformation of the Northern Pelagonian Nappe Pile in the Hellenides. Austrian Journal of Earth Sciences 103, 4–28.
Kjarsgaard, B., Hamilton, D., 1988. Liquid immiscibility and the origin of alkali-poor carbonatites. Mineralogical Magazine 52, 43–55.
Klemme, S., Dalpé, C., 2003. Trace-element partitioning between apatite and carbonatite melt. American Mineralogist 88, 639–646.
Kogarko, L., Zartman, R., 2007. A Pb isotope investigation of the Guli massif, Maymecha-Kotuy alkaline-ultramafic complex, Siberian flood basalt province, Polar Siberia. Mineralogy and petrology 89, 113–132.
Kostopoulos, D.K., James, S.D., 1992. Parameterization of the melting regime of the shallow upper mantle and the effects of variable lithospheric stretching on mantle modal stratification and trace-element concentrations in magmas. Journal of Petrology 33, 665–691.
Larionov, A.N., V.A., A., Gee, D.G., 2004. The Vendian alkaline igneous suite of northern Timan: ion microprobe U–Pb zircon ages of gabbros and syenite. In: Gee, D.G., Pease, V.L. (Eds.), The Neoproterozoic Timanide Orogen of Eastern Baltica. Geological Society of London Members, London, pp. 69–74.
Le Bas, M., 1981. Carbonatite magmas. Mineralogical Magazine 44, 133–140.
Le Bas, M., 1989. In: Bell, K. (Ed.), Diversification of carbonatite Carbonatites, Genesis and Evolution. Unwin Hyman, pp. 428–447.
Le Bas, M., 2008. Fenites associated with carbonatites. The Canadian Mineralogist 46, 915–932.
Le Bas, M., Subbarao, K., Walsh, J., 2002. Metacarbonatite or marble?—the case of the carbonate, pyroxenite, calcite–apatite rock complex at Borra, Eastern Ghats, India. Journal of Asian Earth Sciences 20, 127–140.
Lentz, D.R., 1999. Carbonatite genesis: a reexamination of the role of intrusion-related pneumatolytic skarn processes in limestone melting. Geology 27, 335–338.
Lips, A.L.W., White, S.H., Wijbrans, J.R., 1998. Ar-40/Ar-39 laserprobe direct dating of discrete deformational events: a continuous record of early Alpine tectonics in the Pelagonian Zone, NW Aegean area, Greece. Tectonophysics 298, 133–153.
Ludwig, K.R., 2005a. SQUID 1.12 A User's manual. A Geochronological Toolkit for Microsoft Excel. Berkeley Geochronology Center Spec Pub, 22.
Ludwig, K.R., 2005b. User's manual for ISOPLOT/Ex 3.22. A Geochronological Toolkit for Microsoft Excel. Berkeley Geochronology Center Spec Pub, 71.
Mercier, J., 1968. Etude Géologique des zones Hellénides en Macèdoine centrale (Grece). Ann. Géol. Pays Hell. 20, 17–92.
Millonig, L.J., Gerdes, A., Groat, L.A., 2013. The effect of amphibolite facies metamorphism on the U–Th–Pb geochronology of accessory minerals from meta-carbonatites and associated meta-alkaline rocks. Chemical Geology 353, 199–209.
Mitchell, R.H., 2005. Carbonatites and carbonatites and carbonatites. The Canadian Mineralogist 43, 2049–2068.
Moecher, D.P., Anderson, E.D., Cook, C.A., Mezger, K., 1997. The petrogenesis of metamorphosed carbonatites in the Grenville Province, Ontario. Canadian Journal of Earth Sciences 34 (9), 1185–1201.
Mountrakis, D., 1986. The Pelagonia zone in Greece: a polyphase deformed fragment of the Cimmerian continent and its role in the geotectonic evolution of the Eastern Mediterranean. Journal of Geology 94, 335–347.
Muttoni, G., Gaetani, M., Kent, D.V., Sciunnach, D., Angiolini, L., Berra, F., Garzanti, E., Mattei, M., Zanchi, A., 2009. Opening of the Neo-Tethys Ocean and the Pangea B to Pangea A transformation during the Permian. GeoArabia 14, 17–48.
Nance, D., 1981. Tectonic history of a segment of the Pelagonian zone, northeastern Greece. Canadian Journal of Earth Sciences 18, 1111–1126.
Nelson, D., Chivas, A., Chappell, B., McCulloch, M., 1988. Geochemical and isotopic systematics in carbonatites and implications for the evolution of ocean-island sources. Geochimica et Cosmochimica Acta 52, 1–17.
Patterson, M.V., Francis, D., 2013. Kimberlite eruptions as triggers for early Cenozoic hyperthermals. Geochemistry, Geophysics, Geosystems 14, 448–456.
Pearce, J.A., 1996. A users guide to basalt discrimination diagrams. In: Wyman, D.A. (Ed.), Trace Element Geochemistry of Volcanic Rocks: Applications for Massive Sulphide Exploration. Geological Association of Canada, Canada.
Pe-Piper, G., 1998. The nature of Triassic extension-related magmatism in Greece: evidence from Nd and Pb isotope geochemistry. Geol. Mag. 3, 331–348.
Rajesh, V., Arai, S., 2006. Baddeleyite-apatite-spinel-phlogopite (BASP) rock in Achankovil Shear Zone, South India, as a probable cumulate from melts of carbonatite affinity. Lithos 90, 1–18.
Reguir, E.P., Chakhmouradian, A.R., Pisiak, L., Halden, N.M., Yang, P., Xu, C., Kynický, J., Couëslan, C.G., 2012. Trace-element composition and zoning in clinopyroxene-and amphibole-group minerals: implications for element partitioning and evolution of carbonatites. Lithos 128, 27–45.
Reischmann, T., Kostopoulos, D.K., Loos, S., Anders, B., Avgerinas, A., Sklavounos, S.A., 2001. Late Palaeozoic magmatism in the basement rocks southwest of Mt. Olympos, Central Pelagonian Zone, Greece: remnants of a Permo-Carboniferous magmatic arc. Bulletin of the Geological Society of Greece XXXIV/3, 985–993.
Ricou, L.E., Burg, J.P., Godfriaux, I., Ivanov, Z., 1998. Rhodope and vardar: the metamorphic and the olistostromic paired belts related to the Cretaceous subduction under Europe. Geodinamica Acta 11, 285–309.
Schenker, F.L., Gerya, T., Burg, J.-P., 2012. Bimodal behavior of extended continental lithosphere: Modeling insight and application to thermal history of migmatitic core complexes. Tectonophysics 579, 88–103.
Schenker, F.L., Burg, J.-P., Kostopoulos, D., Moulas, E., Larionov, A., von Quadt, A., 2014. From Mesoproterozoic magmatism to collisional Cretaceous anatexis: tectonomagmatic history of the Pelagonian Zone, Greece. Tectonics 33, 1552–1576.
Schenker, F.L., Fellin, M.G., Burg, J.P., 2015. Polyphase evolution of Pelagonia (northern Greece) revealed by geological and fission-track data. Solid Earth 6, 285–302.
Schermer, E.R., 1990. Mechanisms of blueschist creation and preservation in an a-type subduction zone, Mount-Olympus Region, Greece. Geology 18, 1130–1133.
Schermer, E.R., Lux, D.R., Burchfiel, B.C., 1990. Temperature-time history of subducted continental-crust, Mount Olympos Region, Greece. Tectonics 9, 1165–1195.
Sharp, Z., 2007. Principle of Stable Isotope Geochemistry. Pearson Prentice Hall, Upper Saddle River, NJ.
Sharp, I.R., Robertson, A.H.F., 2006. Tectonicsedimentary evolution of the western margin of the Mesozoic Vardar Ocean: evidence from the Pelagonian and Almopias zones, northern Greece. In: Robertson, A.H.F., Mountrakis, D. (Eds.), Tectonic Development of the Eastern Mediterranean Region. Geological Society, London, pp. 373–412.
Song, W.L., Xu, C., Veksler, I.V., Kynicky, J., 2016. Experimental study of REE, Ba, Sr, Mo and W partitioning between carbonatitic melt and aqueous fluid with implications for rare metal mineralization. Contrib Mineral Petrol 171, 1.
Spear, F.S., Kohn, M.J., Florence, F.P., Menard, T., 1990. A model for garnet and Plagioclase growth in pelitic schists - implications for thermobarometry and P-T path determinations. Journal of Metamorphic Geology 8, 683–696.
Stamfli, G.M., Kozur, H.W., 2006. Europe from the Variscan to the Alpine Cycles Geological Society of London.
Steiger, R.J., Jäger, E., 1977. Subcommission on geochronology: convention on the use of decay constants in geo- and cosmo-chronology. Earth Planet Sci Lett 36, 4.
Streckeisen, A., 1980. Classification and nomenclature of volcanic rocks, lamprophyres, carbonatites and melilitic rocks IUGS Subcommission on the systematics of igneous rocks. Geologische Rundschau 69, 194–207.
Sun, S.S., McDonough, W.F., 1989. Chemical and isotopic systematics of oceanic basalts; implications for mantle composition and processes. In: Saunders, A.D., Norry, M.J. (Eds.), Magmatism in the Ocean Basins. Geological Society of London, London, pp. 313–345.
Tappe, S., Romer, R.L., Stracke, A., Steenfelt, A., Smart, K.A., Muehlenbachs, K., Torsvik, T.H., 2017. Sources and mobility of carbonate melts beneath cratons, with implications for deep carbon cycling, metasomatism and rift initiation. Earth and Planetary Science Letters 466, 152–167.
Teipel, U., Eichhorn, R., Loth, G., Rohrmuller, J., Holl, R., Kennedy, A., 2004. U-PbSHRIMP and Nd isotopic data from the western Bohemian Massif (Bayerischer Wald, Germany): implications for Upper Vendian and Lower Ordovician magmatism. International Journal of Earth Sciences 93, 782–801.
Tera, F., Wasserburg, G.J., 1972. U-Th-Pb Systematics in 3 Apollo 14 Basalts and Problem of Initial Pb in Lunar Rocks. Earth and Planetary Science Letters 14, 281-&.
Valley, J.W., 2003. Oxygen isotopes in zircon. Reviews in Mineralogy and Geochemistry 53, 343–385.
Valley, J.W., Kinny, P.D., Schulze, D.J., Spicuzza, M.J., 1998. Zircon megacrysts from kimberlite: oxygen isotope variability among mantle melts. Contributions to Mineralogy and Petrology 133, 1–11.
Vladykin, N., 2016. Genesis and crystallization of ultramafic alkaline carbonatite magmas of Siberia: ore potential, mantle sources, and relationship with plume activity. Russian Geology and Geophysics 57, 698–712.
Walter, M., Bulanova, G., Armstrong, L., Keshav, S., Blundy, J., Gudfinnsson, G., Lord, O., Lennie, A., Clark, S., Smith, C., 2008. Primary carbonatite melt from deeply subducted oceanic crust. Nature 454, 622–625.
Watkinson, D.H., Wyllie, P.J., 1971. Experimental study of the composition join $NaAlSiO_4$-$CaCO_3$-H_2O and the genesis of Alkalic Rock—carbonatite complexes. Journal of Petrology 12, 357–378.
Watson, E., Cherniak, D., 1997. Oxygen diffusion in zircon. Earth and Planetary Science Letters 148, 527–544.
Weidendorfer, D., Schmidt, M.W., Mattsson, H.B., 2016. Fractional crystallization of Si-undersaturated alkaline magmas leading to unmixing of carbonatites on Brava Island (Cape Verde) and a general model of carbonatite genesis in alkaline magma suites. Contributions to Mineralogy and Petrology 171, 1–29.

Wetherill, G.V., 1956. Discordant uranium-lead ages. I. Trans American Geoph Union 37, 320–326.
Williams, I.S., 1998. U-Th-Pb geochronology by ion microprobe. In: McKibben, M.A., Shanks, W.C., W.I., R. (Eds.), Applications of Microanalytical Techniques to Understanding Mineralizing Processes. Reviews Economic Geology, pp. 1–35.
Wilson, M., 1989. Igneous Petrogenesis, London.
Winchester, J.A., Floyd, P.A., 1977. Geochemical discrimination of different magma series and their differentiation products using immobile elements. Chemical Geology 20, 325–343.
Woolley, A.R., 1989. The spatial and temporal distribution of carbonatites. In: Bell, K. (Ed.), Carbonatites - Genesis and Evolution. Unwin Hyman, London, pp. 15–37.
Woolley, A.R., Kempe, D.R.C., 1989. Carbonatites: nomenclature, average chemical compositions, and element distribution. In: Bell, K. (Ed.), Carbonatites - Genesis and Evolution. Unwin Hyman, London, pp. 1–37.
Woolley, A.R., Kjarsgaard, B.A., 2008. Carbonatite occurrences of the world: map and database Geological Survey of Canada.
Woolley, A., Barr, M., Din, V., Jones, G., Wall, F., Williams, C., 1991. Extrusive carbonatites from the Uyaynah area, United Arab Emirates. Journal of Petrology 32, 1143–1167.
Wyllie, P., 1989. Origin of carbonatites: evidence from phase equilibrium studies. Carbonatites: Genesis and Evolution. Unwin Hyman, London, pp. 500–545.
Xu, C., Kynicky, J., Chakhmouradian, A.R., Campbell, I.H., Allen, C.M., 2010. Trace-element modeling of the magmatic evolution of rare-earth-rich carbonatite from the Miaoya deposit, Central China. Lithos 118, 145–155.
Xu, C., Taylor, R.N., Kynicky, J., Chakhmouradian, A.R., Song, W., Wang, L., 2011. The origin of enriched mantle beneath North China block: evidence from young carbonatites. Lithos 127, 1–9.
Xu, C., Kynicky, J., Chakhmouradian, A.R., Li, X., Song, W., 2015. A case example of the importance of multi-analytical approach in deciphering carbonatite petrogenesis in South Qinling orogen: Miaoya rare-metal deposit, central China. Lithos 227, 107–121.
Yang, K.-F., Fan, H.-R., Santosh, M., Hu, F.-F., Wang, K.-Y., 2011. Mesoproterozoic carbonatitic magmatism in the Bayan Obo deposit, Inner Mongolia, North China: constraints for the mechanism of super accumulation of rare earth elements. Ore Geology Reviews 40, 122–131.
Yarwood, G.A., Dixon, J.E., 1977. Lower Cretaceous and younger thrusting in the Pelagonian rocks of high Piera, Greece. 6th Colloq. Aegean Region, Athens. 1, pp. 269–280.
Zlatkin, O., Avigad, Z., Gerdes, A., 2017. The Pelagonian terrane of Greece in the peri-Gondwanan mosaic of the Eastern Mediterranean: implications for the geological evolution of Avalonia. Precambrian Research 290, 163–183.